POLITECNICO DI TORINO
Repository ISTITUZIONALE

Coupled thermo-mechanical finite element models with node-dependent kinematics for multi-layered shell structures

(Article begins on next page)

29 November 2022

Coupled thermo-mechanical finite element models with node-dependent kinematics for multi-layered shell structures

G. Li[a,*], M. Cinefra[a,], E. Carrera[a,]

[a]*MUL²* *Group, Department of Mechanical and Aerospace Engineering, Politecnico di Torino,*
Corso Duca degli Abruzzi 24, 10129 Torino, Italy.

Abstract

Node-dependent Kinematics (NDK) shell finite element (FE) formulations are presented for the steady-state thermo-mechanical analysis of laminated structures. The displacements and temperature change are treated as primary variables in the FE models and are directly solved through the coupled thermo-mechanical models. The enforcement of distributed temperature boundary conditions on the top or the bottom surfaces of hierarchical shell elements is conducted through the Linear Least Squares. The effectiveness of the proposed FE approaches is verified by comparing the results against those from the literature. The application of adaptive refinement approach based on the hierarchical elements and NDK to build FE models with optimal efficiency is demonstrated through a numerical example.

Keywords: thermal stresses, node-dependent kinematics, composite shells, hierarchical element, Carrera Unified Formulation

1. Introduction

Stresses due to temperature variation are important environmental effects on composite structures. In laminated shells, thermal stresses may induce matrix cracks or delaminations. In finite element (FE) simulations, accurate thermal stress evaluations require reliable temperature estimation and proper thermo-mechanical coupling.

Heat conduction is governed by the Fourier law of conduction [10]. The resultant temperature variation causes strains in structures. Due to the thermo-mechanical coupling, straining of structures also generates heat in transient and dynamic processes. In steady-state conditions, thermo-mechanical problems are partially coupled, which means only the deformation due to

---

*Corresponding author. Tel: +39 0110906870, Fax: +39 0110906899.
Email address: guohong.li@polito.it (G. Li)

temperature change is considered. Most works available in the literature adopt assumed temperature field. Das and Rath [7] considered the transverse shear effects in the bending of a thick plate under the assumed temperature field. Miller et al. [23] reported the use of Kirchoff-Love hypothesis in layered shell models, and the temperature variation was taken as input to the analysis. Kant and Khare [13] used a higher-order model in FE modeling of multi-layered plates under assumed linear temperature profile through the thickness. Adopting Reddy's higher-order theory [24, 27], Khdeir and Reddy [17], Khare et al. [15] studied the response of cross-ply laminated plates and shell under thermal fields with linear distribution through the thickness and presented exact solutions, respectively. Khdeir [16] suggested closed-form solutions for circular cylindrical shells under temperature field that has assumed uniform or linear variation through the thickness. Based on a higher-order theory [26], Khdeir et al. [18] proposed exact solutions for cylindrical and doubly-curved shells under assumed thermal loads and various boundary conditions.

Temperature field can be obtained in a separate step by solving Fourier's equation and then be used in a subsequent step on the structure as input data. Dumir et al. [8] used an improved efficient zig-zag theory and a third order theory for cylindrical laminated shells, and the exact temperature profile described in a sub-layerwise manner was the input to the partially-coupled thermo-mechanical models. Carrera [1] compared the structural response of multi-layered plates under assumed linear and exact temperature profiles through the thickness and pointed out that the exact temperature field is essential for thick plates. Cinefra et al. [5] developed shell finite elements for the thermoelastic analysis of multi-layered structures under exact temperature fields obtained in a separate step.

Carrera Unified Formulation (CUF) is a general framework for the development of refined plate and shell models proposed by Carrera [4]. Starting from a compact form of displacement assumptions, weak form governing equations can be expressed through the *fundamental nuclei* (FNs) [4]. The expressions of FNs are independent of the kinematic assumptions and are widely applicable to a variety of structural models. CUF framework facilitates the development of advanced FE models. A variety of basis functions can be employed in either ESL (Equivalent-Single Layer) or LW (Layer-Wise) approach to formulating refined structural theories [4]. In CUF-based structural models, the type of basis functions adopted and the number of thickness functions are both variable and can be treated as model input parameters. The refinement of the models can be gradually conducted until the prescribed accuracy is achieved. Besides the refinement of kinematic assumptions, the shape functions can also be enhanced through

p-refinement in hierarchical shell elements. As reported, p-refinement is more efficient than h-refinement due to its high convergence rate [32, 30]. Also, the avoidance of re-meshing can
shorten the pre-processing time consumption. Moreover, it is reported that 2D hierarchical elements are not sensitive to locking phenomena when the polynomial order is sufficiently high [31, 32, 29, 28, 9, 30]

Based on CUF, Carrera and Zappino [2] introduced the dependence of kinematic assumptions on the shape functions in refined FE models. This approach was named as Node-dependent Kinematics (NDK). Trough NDK, various kinematic models can coexist in a shell element and be blended by the shape functions over the shell in-plane domain. More importantly, NDK allows for the local kinematic refinement in the critical region with local effects to be captured. The features make NDK feasible in the construction of simultaneous global-local models with multiple kinematic models [22]. Since no additional coupling or modification of mesh is needed, NDK is convenient to use in FE analyses. In general, the solution accuracy can be improved by enriching the assumptions of the displacement field. Meanwhile, the increased number of model variables leads to raised computational costs in FE analyses. With NDK technique, accuracy in the local area can be kept with lower computational efforts. Li et al. [22] demonstrated that in comparison with 3D elements, the NDK-based refined shell elements have much higher numerical efficiency while guaranteeing the 3D solution accuracy in the local region.

In the present work, the NDK technique is extended to partially coupled steady-state thermo-mechanical simulations. p-version hierarchical shape functions are applied to the shell elements, and FE models with variable ESL/LW nodal capabilities is adopted in the numerical analysis. Hierarchical Legendre Expansions are employed as basis functions of the refined LW models and used in combination with Taylor-type kinematic higher-order models. An adaptive refinement procedure based on NDK to obtain accurate approximates of structural responses is presented, and the numerical efficiency of the proposed approach is demonstrated through numerical examples on laminated shell structures.

2. Preliminaries

Fig. 1 shows a differential element of a shell [25], in which α and β indicate the lines of curvature on the middle surface and z the thickness direction. The infinitesimal area dS parallel to the middle surface at z is:

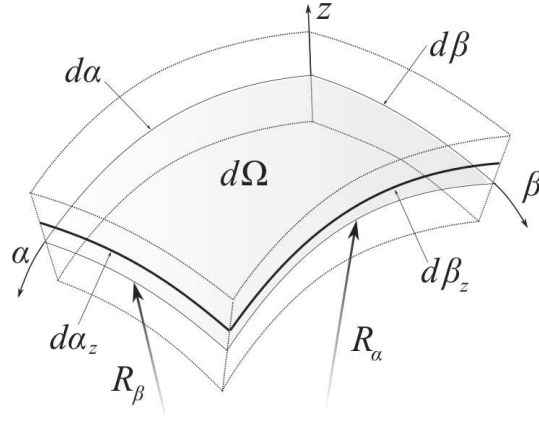$$dS = H_\alpha H_\beta d\alpha d\beta = H_\alpha H_\beta d\Omega \tag{1}$$

3

Figure 1: A differential element of a doubly curved shell structure. R_α and R_β are the radii of curvatures in α and β directions, respectively. $d\Omega$ is the infinitesimal area on the middle surface.

in which $d\Omega$ is the infinitesimal area on the middle surface of the shell. An elemental volume dV is given by:

$$dV = H_\alpha \, H_\beta \, H_z \, d\alpha \, d\beta \, dz \ . \tag{2}$$

For shells with constant radii of curvature, the metric coefficients H_α, H_β, and H_z read:

$$H_\alpha = (1 + z/R_\alpha), \quad H_\beta = (1 + z/R_\beta), \quad H_z = 1 \ . \tag{3}$$

70   where R_α and R_β are the principal radii of curvature of the middle surface. For more details about shell theories, the reader is referred to the works of Leissa [20], Reddy [25].

For doubly curved shells, corresponding to the displacement vector $\boldsymbol{u}(\alpha, \beta, z) = \{u, v, w\}^\top$, the strain vector is arranged as:

$$\boldsymbol{\varepsilon} = \{\varepsilon_{\alpha\alpha}, \varepsilon_{\beta\beta}, \varepsilon_{zz}, \varepsilon_{\beta z}, \varepsilon_{\alpha z}, \varepsilon_{\alpha\beta}\}^\top \tag{4}$$

and the strain components can be obtained by considering:

$$\boldsymbol{\varepsilon} = \mathbf{b}\,\boldsymbol{u} \tag{5}$$

4

in which the differential operator matrix $\mathbf{b}$ reads:

$$
\mathbf{b} =
\begin{bmatrix}
\frac{\partial_\alpha}{H_\alpha} & 0 & \frac{1}{H_\alpha R_\alpha} \\
0 & \frac{\partial_\beta}{H_\beta} & \frac{1}{H_\beta R_\beta} \\
0 & 0 & \partial_z \\
0 & \partial_z - \frac{1}{H_\beta R_\beta} & \frac{\partial_\beta}{H_\beta} \\
\partial_z - \frac{1}{H_\alpha R_\alpha} & 0 & \frac{\partial_\alpha}{H_\alpha} \\
\frac{\partial_\beta}{H_\beta} & \frac{\partial_\alpha}{H_\alpha} & 0
\end{bmatrix}
\tag{6}
$$

Note that when $H_\alpha = H_\beta = 1$ ($R_\alpha \to \infty$, $R_\beta \to \infty$), a shell becomes a plate which is flat in geometry.

The temperature gradient vector $\boldsymbol{\vartheta}$ can be obtained through:

$$
\boldsymbol{\vartheta} = -\nabla\theta
\tag{7}
$$

where ∇ is the gradient operator vector. For doubly curved shells, ∇ takes the following form:

$$
\nabla = \{\frac{\partial_\alpha}{H_\alpha}, \frac{\partial_\beta}{H_\beta}, \partial_z\}^\top
\tag{8}
$$

For a homogeneous medium, the linear constitutive relations in matrix form read:

$$
\boldsymbol{\sigma} = \boldsymbol{C}\boldsymbol{\varepsilon} - \boldsymbol{\lambda}^\top\theta
\tag{9}
$$

$$
\boldsymbol{q} = \boldsymbol{\kappa}\boldsymbol{\vartheta}
\tag{10}
$$

wherein $\boldsymbol{\sigma}$ is the stress vector, $\boldsymbol{q}$ the heat flux vector, and $\boldsymbol{\lambda}$ the thermal stress coefficients vector. For shells with double curvatures, $\boldsymbol{\sigma}$ is arranged as:

$$
\boldsymbol{\sigma} = \{\sigma_{\alpha\alpha}, \sigma_{\beta\beta}, \sigma_{zz}, \sigma_{\beta z}, \sigma_{\alpha z}, \sigma_{\alpha\beta}\}^\top
\tag{11}
$$

In orthotropic materials, there exist three orthogonal planes of symmetry. In the material

5

coordinate system $(1, 2, 3)$, the material coefficient matrix $\boldsymbol{C}_m$ takes the following form:

$$\boldsymbol{C}_m = \begin{bmatrix} C_{11} & C_{12} & C_{13} & 0 & 0 & 0 \\ C_{21} & C_{22} & C_{23} & 0 & 0 & 0 \\ C_{31} & C_{32} & C_{33} & 0 & 0 & 0 \\ 0 & 0 & 0 & C_{44} & 0 & 0 \\ 0 & 0 & 0 & 0 & C_{55} & 0 \\ 0 & 0 & 0 & 0 & 0 & C_{66} \end{bmatrix} \tag{12}$$

which is characterized by nine independent material constants, namely the Young's moduli (E_1, E_2, E_3), the shear moduli (G_{23}, G_{13}, G_{12}), and the Poisson ratios (ν_{12}, ν_{13}, ν_{23}). For more details, one is referred to the work of Reddy [25].

The heat conduction coefficient matrix $\boldsymbol{\kappa}_m$ in the material coordinates reads:

$$\boldsymbol{\kappa}_m = \begin{bmatrix} \kappa_{11} & 0 & 0 \\ 0 & \kappa_{22} & 0 \\ 0 & 0 & \kappa_{33} \end{bmatrix} \tag{13}$$

Temperature increase causes the structure to expand and results in the change of stresses. This effect is captured by the thermal stress coefficients vector $\boldsymbol{\lambda}$. Expressed in the material coordinate system $(1, 2, 3)$, $\boldsymbol{\lambda}_m$ has the following relation with the thermal expansion coefficients $\boldsymbol{\alpha}_m$:

$$\boldsymbol{\lambda}_m^\top = \boldsymbol{C}_m \, \boldsymbol{\alpha}_m \tag{14}$$

wherein

$$\boldsymbol{\alpha}_m = \left\{ \alpha_{11} \quad \alpha_{22} \quad \alpha_{33} \quad 0 \quad 0 \quad \alpha_{12} \right\}^\top \tag{15}$$

For the transformation of the material coefficient matrices from the material coordinate system to the analysis system, the reader is referred to Li [21].

3. Node-dependent Kinematic shell FE models

Based on CUF, the displacements of a plate structure can be approximated as:

$$\boldsymbol{u}(x, y, z) = F_\tau(z) \boldsymbol{u}_\tau(x, y) \tag{16}$$

6

where the thickness functions $F_\tau(z)$ are determined by the adopted theories of shell structures, and $\boldsymbol{u}_\tau(x, y)$ are the in-plane displacement vectors. As presented by Carrera et al. [4], both ESL and LW models for laminated shells can be considered in the CUF framework.

In FE models with Node-dependent Kinematics (NDK):

$$
\begin{aligned}
\boldsymbol{u}(x, y, z) &= F_\tau^i(z) N_i(x, y) \boldsymbol{u}_{i\tau} \\
\delta\boldsymbol{u}(x, y, z) &= F_s^j(z) N_j(x, y) \delta\boldsymbol{u}_{js}
\end{aligned}
\tag{17}
$$

in which δ denotes the virtual variation, and $F_\tau^i(z)$ and $F_\tau^j(z)$ represent kinematic assumptions defined on node i and j, respectively. In a further step, general expressions of the stiffness matrix and the load vector of the FE models, the *Fundamental Neuclei* (FNs), can be obtained by applying the Principle of Virtual Displacements (PVD). Some examples of FNs have been given by Carrera et al. [4].

In LW-type kinematic models, thickness functions are expressed by using the non-dimensional thickness coordinate ζ in each layer. In the present work, the 1D hierarchical Legendre Expansions (HLE) are adopted as thickness functions in the LW framework. The explicit expressions of thickness functions adopting 1D HLE are:

$$
F_\tau(\zeta) = \begin{cases}
\dfrac{1}{2}(1 - \zeta) & \tau = 0 \\[2mm]
\dfrac{1}{2}(1 + \zeta) & \tau = 1 \\[2mm]
\sqrt{\dfrac{2\tau - 1}{2}} \displaystyle\int_{-1}^{\zeta} L_{\tau-1}(x)dx = \dfrac{L_\tau(\zeta) - L_{\tau-2}(\zeta)}{\sqrt{4\tau - 2}} & \tau = 2, 3, \cdots
\end{cases}
\tag{18}
$$

in which $L_\tau(\delta)$ are the Legendre polynomials. Such basis functions in Eqn. 18 are also adopted in the construction of the 2D hierarchical (p-version) elements (see references [32, 30]).

4. Coupled thermo-mechanical shell FE models

4.1. Weak-form governing equations

For a unit volume in the kth layer of the laminated shell, by applying PVD, one has:

$$
\delta E_p = \delta W
\tag{19}
$$

in which:

$$
\delta E_p = \int_V (\boldsymbol{\sigma}^{k\top} \delta\boldsymbol{\varepsilon}^k - \boldsymbol{q}^{k\top} \delta\boldsymbol{\vartheta}^k)dV
\tag{20}
$$

7

$$\delta W = \int_\Gamma (\delta \boldsymbol{u}^{k\top} \bar{\boldsymbol{p}} + \delta\theta^k \, \bar{q}_n) \, d\Gamma \tag{21}$$

wherein E_p represents the potential energy, W the external work, $\boldsymbol{p}$ the surface traction vector, q_n the normal heat flux, and h_n the normal moisture flux. For steady-state cases, the inertial work is discarded.

The approximations of the primary variables are:

$$\boldsymbol{u}^k = N_i \, F_\tau^{i\,k} \, \boldsymbol{u}_{i\tau}^{(k)}, \qquad \delta\boldsymbol{u}^k = N_j \, F_s^{j\,k} \delta\boldsymbol{u}_{js}^{(k)}. \tag{22}$$

$$\theta^k = N_i \, F_\tau^{i\,k} \theta_{i\tau}^{(k)}, \qquad \delta\theta^k = N_j \, F_s^{j\,k} \delta\theta_{js}^{(k)}. \tag{23}$$

in which for ESL models $\boldsymbol{u}_{i\tau}^{(k)} = \boldsymbol{u}_{i\tau}$, and for LW models $\boldsymbol{u}_{i\tau}^{(k)} = \boldsymbol{u}_{i\tau}^k$. This rule also applies to other variables.

The essential boundary conditions are considered through:

$$N_i \, F_\tau^{i\,k} \, \bar{\boldsymbol{u}}_{i\tau}^{(k)} = \overline{\boldsymbol{u}} \quad \text{on } \Gamma_{\boldsymbol{u}}, \qquad N_i \, F_\tau^{i\,k} \, \bar{\theta}_{i\tau}^{(k)} = \overline{\theta} \quad \text{on } \Gamma_\theta. \tag{24}$$

By considering the above FE approximations, the strain-displacement relations in Eqn. 5, the gradient equations in Eqn. 7, and the constitutive relations in Eqn. 9, one can obtain:

$$\begin{aligned}
\delta\boldsymbol{u}_{js}^{(k)\top} : &\quad \boldsymbol{K}_{ij\tau s}^{\boldsymbol{uu}\,k} \boldsymbol{u}_{i\tau}^{(k)} + \boldsymbol{K}_{ij\tau s}^{\boldsymbol{u\theta}\,k} \theta_{i\tau}^{(k)} = \boldsymbol{P}_{js}^{\boldsymbol{u}\,k} \\
\delta\theta_{js}^{(k)} : &\quad \qquad\qquad K_{ij\tau s}^{\theta\theta\,k} \theta_{i\tau}^{(k)} = P_{js}^{\theta\,k}
\end{aligned} \tag{25}$$

and the *fundamental nuclei* (FNs) of the generalized stiffness matrices are:

$$\boldsymbol{K}_{ij\tau s}^{\boldsymbol{uu}\,k} = \int_\Omega \int_{A^k} (\mathbf{b} \, N_j F_s^{j\,k})^\top \boldsymbol{C}^k (\mathbf{b} \, N_i F_\tau^{i\,k}) H_\alpha H_\beta dz^k d\Omega \tag{26}$$

$$\boldsymbol{K}_{ij\tau s}^{\boldsymbol{u\theta}\,k} = -\int_\Omega \int_{A^k} (\mathbf{b} \, N_j F_s^{j\,k})^\top \boldsymbol{\lambda}^{k\top} (N_i F_\tau^{i\,k}) H_\alpha H_\beta dz^k d\Omega \tag{27}$$

$$K_{ij\tau s}^{\theta\theta\,k} = -\int_\Omega \int_{A^k} (\nabla \, N_j F_s^{j\,k})^\top \boldsymbol{\kappa}^k (\nabla \, N_i F_\tau^{i\,k}) H_\alpha H_\beta dz^k d\Omega \tag{28}$$

in which A^k is the thickness domain of the kth layer and Ω the element in-plane domain on the

middle surface. For examples of FNs for refined shell models, the reader is referred to the work of Li et al. [22].

External loads caused by the essential boundary conditions can be considered as:

$$\boldsymbol{P}_{js}^{\bar{u}\ k} = -\boldsymbol{K}_{ij\tau s}^{\boldsymbol{uu}\ k} \bar{\boldsymbol{u}}_{i\tau}^{(k)} - \boldsymbol{K}_{ij\tau s}^{\boldsymbol{u\theta}\ k} \bar{\theta}_{i\tau}^{(k)} \tag{29}$$

$$P_{js}^{\bar{\theta}\ k} = -K_{ij\tau s}^{\theta\theta\ k} \bar{\theta}_{i\tau}^{(k)} \tag{30}$$

FNs for the loads due to natural boundary conditions read:

$$\boldsymbol{P}_{js}^{\bar{p}\ k} = \int_{\Gamma_p} N_j F_s \bar{\boldsymbol{p}} d\Gamma \quad \text{on } \Gamma_p \tag{31}$$

$$P_{js}^{\bar{q}\ k} = \int_{\Gamma_q} N_j F_s \bar{q}_n d\Gamma \quad \text{on } \Gamma_q \tag{32}$$

Since the boundary conditions mentioned above are imposed on different external sub-surfaces, their load vectors can be assembled separately then summed up as:

$$\boldsymbol{P}^{\boldsymbol{u}} = \boldsymbol{P}^{\bar{u}} + \boldsymbol{P}^{\bar{p}} \tag{33}$$

$$\boldsymbol{P}^{\theta} = \boldsymbol{P}^{\bar{\theta}} + \boldsymbol{P}^{\bar{q}} \tag{34}$$

100   The generalized stiffness matrix and load vector need to be assembled within each element, then on the whole FE model level. The assembly technique of CUF-based FE models has been elaborated by Li [21].

4.2. Enforcement of temperature boundary conditions

To impose distributed temperature on the top or the bottom surfaces of hierarchical shell elements, one needs to consider:

$$\bar{\theta}(\alpha, \beta) = N_i(\alpha, \beta)\, \bar{\theta}_i \tag{35}$$

For shell elements adopting Lagrangian interpolation polynomials, since the nodal unknown $\bar{\theta}_i$ is
105   the exact value of the temperature field, it is straightforward to impose the above boundary con-

ditions on FE models. However, for hierarchical elements, $\bar{\theta}_i$ are merely mathematical weighting coefficients which need to be calculated to approximate the temperature boundary conditions to be enforced.

The procedure to calculate $\bar{\theta}_i$ for hierarchical shell elements is, in essence, a curve-fitting problem. To guarantee the approximation accuracy, the number of essential sampling points should be higher than the number of shape functions. In the present work, these unknowns are obtained through the Linear Least Squares (LLS). For hierarchical elements of order p, besides the four vertex nodes, the number of equally-spaced sampling points in each direction in the in-plane domain is chosen to be $p+4$. After $\bar{\theta}_i$ are obtained, by considering Eqn. 30, the temperature boundary conditions can be imposed on the FE models.

4.3. Adaptive refinement

The order of the elements and nodal kinematic assumptions are refined adaptively. The order of the hierarchical elements, the kinematic assumptions in the local critical region, the area of the local region, and the kinematic models refined in the non-critical zone, are one-by-one gradually enhanced or enlarged until the desired relative difference between two consecutive simulation rounds is reached.

In the current work, the numerical convergence threshold δ is chosen to be 1%, which means that the mathematical enhancement of the FE models stops when:

$$\max\left(\left|\frac{u_i^{(M)} - u_i^{(M-1)}}{u_i^{(M)}}\right|, \left|\frac{\sigma_{ij}^{(M)} - \sigma_{ij}^{(M-1)}}{\sigma_{ij}^{(M)}}\right|\right) \leq \delta \quad i = 1, 2, 3. \tag{36}$$

in which M is the current round of simulation.

5. Results and discussion

In this section, the adopted FE models are first validated by comparing the FE results with those obtained through analytical solutions for three example of multi-layered shells, then a two-layered spherical shell with local distributed temperature is simulated with NDK shell FE models. The numerical efficiency is assessed through the number of DOFs used and CPU time consumed. The distributed temperature boundary conditions are enforced on the hierarchical shell elements through the LLS approach.

10

5.1. Heat conduction in hybrid five-layered cross-ply cylindrical shells

Hybrid five-layered cylindrical shells are considered in the first numerical example, which focuses on the heat conduction simulation. The laminated shells, with the stacking sequence [PVDF/90°/0°/90°/PVDF], consist of a core with three equal-thickness graphite-epoxy layers and two external faces made of polyvinylidene fluoride (PVDF). Each PVDF layer takes one-tenth of the total thickness, thus the ply thickness follows $[\frac{h_0}{10}/\frac{4h_0}{15}/\frac{4h_0}{15}/\frac{4h_0}{15}/\frac{h_0}{10}]$. The thermal conductivities of the graphite-epoxy are $k_{11} = 36.42\text{W/mK}$, $k_{22} = k_{33} = 0.96\text{W/mK}$, and of the PVDF layers $k_{11} = k_{22} = k_{33} = 0.24\text{W/mK}$. The axial length of the cylindrical shells is $L = 4\text{m}$ and the radius $R = 1\text{m}$. The temperature rise on the bottom of the shells is constraint to be $\theta(-\frac{h}{2}) = 0$, and on the top surface, the imposed temperature follows:

$$\theta(\alpha, \beta, \frac{h}{2}) = \theta_0 \cdot \sin(\frac{\pi\alpha}{L}) \tag{37}$$

in which $\theta_0 = 1\text{K}$.

Single-element FE models consisting of p-version shell elements with refined kinematics are built. Radius-to-thickness ratios $R/h = 2, 4$, and 100 are considered. By increasing the element order and refining the kinematic assumptions gradually and considering a convergence threshold
of $\delta = 0.01\%$ for the temperature, $p5$-HLP3 (fifth-order p-version element and third-order Legendre polynomials as thickness functions in the LW framework) has been chosen to provide the numerical estimation of temperature. Table 1 reports a comparison of the obtained temperature against reference solutions given by Kapuria et al. [14], Kulikov and Plotnikova [19], and Fig. 2 shows the through-thickness variation of temperature. It can be observed that the obtained
numerical results agree well with the reference solutions.

Table 1: Temperature rise in the five-layered cylindrical shell at $L/2$ and $\bar{z} = \pm 0.4$.

	$\bar{z} = -0.4$		$\bar{z} = 0.4$	
R_β/h	4	100	4	100
Present	0.2398	0.2511	0.7385	0.7511
Kapuria et al. [14]	0.2398	0.2511	0.7385	0.7511
Kulikov and Plotnikova [19]	0.23984	0.25106	0.73853	0.75106

5.2. Spherical sandwich shell under the temperature field with a linear through-thickness profile

This numerical example emphasizes on the thermo-mechanical coupling effects. The simply supported sandwich shells considered have the lamination sequence [0°/core/0°], and the material
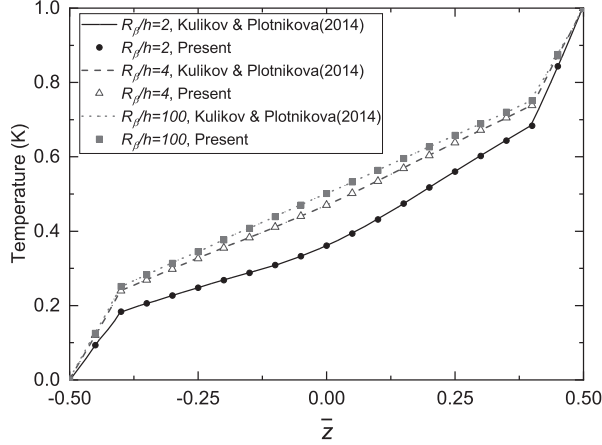
Figure 2: Through-thickness variation of temperature on the hybrid five-layered cylindrical shells with polyvinyli-dene fluoride (PVDF) layers. Numerical results obtained with the employed FE models are compared against the reference solutions.

properties are as in Table 2. The composite faces have equal thickness $0.1h$, where h is the total thickness of the shells. The lengths of the edges are $a = b = 1$m, and the radii of in the two in-plane direction are equal, which means $R_\alpha = R_\beta = R$. Radius-to-thickness ratios $R/h = 5$, 10, 20 and ∞ (plate) are considered, and the length-to-thickness ratio analyzed include $a/h = 4$ and 100. The assumed temperature field has a linear profile through the shell thickness and bi-sinusoidal in-plane distribution which means:

$$\theta(\alpha, \beta, z) = (T_0 + \frac{z}{h}T_1) \cdot \sin(\frac{\pi\alpha}{a})\sin(\frac{\pi\beta}{b}) \tag{38}$$

where $T_0 = 0$K and $T_1 = 1$K. As a result, the imposed temperature on the top surface is 0.5K and the bottom surface -0.5K. The adopted simply supported boundary conditions are:

$$\begin{aligned}\alpha = 0, a : \quad v = 0, w = 0, \theta = 0; \\ \beta = 0, b : \quad u = 0, w = 0, \theta = 0.\end{aligned} \tag{39}$$

Table 2: Mechanical properties of the faces and core on the spherical sandwich shells.

	E_1 (GPa)	E_2, E_3 (GPa)	G_{12}, G_{13} (GPa)	G_{23} (GPa)	$\nu_{12}, \nu_{13}, \nu_{23}$	α_{22} $(10^{-6}/K)$	α_{11}, α_{33} $(10^{-6}/K)$
Faces	172.37	6.89	3.45	1.38	0.25	20.0	1.0
Core	0.28	3.45	0.11	0.41	0.25	2.0	0.1

A quarter of the structure is simulated by single-element FE models employing p-elements

and higher-order Legendre-type kinematics (HLE). Based on the convergence study, the FE model $p11$-HLE5 is chosen to provide the numerical results. The obtained numerical estimation of the deflection at the centroid of the shells have been summarized in Table 3. For comparison purposes, the results provided by Carrera et al. [3] using closed-form solutions based on LD4 (fourth-order Lagrange polynomials as thickness functions) and by Khare et al. [15] with a higher-order deformation model HOST12 have also been listed. A high agreement between the present results and the reference solutions can be observed, which demonstrates that the thermo-mechanical coupling effects are appropriately considered in the proposed models.

Table 3: Displacement estimations on the spherical sandwich shells under the temperature field with a linear through-thickness profile.

R/h		5	10	20	Plate
	Present	4.3496	4.3730	4.3789	4.3809
$a/h = 4$	LD4 [3]	4.3426	4.3657	4.3715	4.3735
	HOST12 [15]	4.2032	4.2343	4.2422	4.2448
	Present	0.8630	1.4111	1.6767	1.7890
$a/h = 100$	LD4 [3]	0.8637	1.4118	1.6774	1.7896
	HOST12 [15]	0.8780	1.4368	1.7077	1.8221

5.3. Composite cylindrical panels with imposed temperature on top and bottom surfaces

Two-layered cylindrical panels with lamination sequence [0°/90°] (from bottom to top, with equal thickness) under enforced temperature on the external surfaces are studied. The dimensions of the cylindrical panels are: length and width $a = b = 0.1$m, radii $R_\alpha = 0.1$m and $R_\beta = \infty$. Radius-to-thickness ratios $R_\alpha/h = 2, 10$ and 500 are investigated. On the bottom surface, the imposed temperature is $\theta_0(\alpha, \beta, -\frac{h}{2}) = 0$K, and on the top surface $\theta_0(\alpha, \beta, \frac{h}{2})$ follows:

$$\theta_0(\alpha, \beta, \frac{h}{2}) = \theta_M \cdot \sin(\frac{\pi\alpha}{a}) \sin(\frac{\pi\beta}{b}) \tag{40}$$

in which $\theta_M = 50$K. The panels are simply supported, and the boundary conditions follow Eqn. 39.

The mechanical and thermal properties of the lamina, set by referring to the work of Jacquemin and Vautrin [12], are given in Table 4 . The heat conduction coefficients (κ_{11}, κ_{22}, and κ_{33}) are assumed with reference to the work of Hicks [11].

With the help of the symmetric boundary conditions, a quarter of the shell is simulated by single-element models employing a hierarchical shell element. The convergence error threshold

13

Table 4: Mechanical properties of T300/5208 composite lamina.

E_1 (GPa)	E_2, E_3 (GPa)	G_{12}, G_{13} (GPa)	G_{23} (GPa)	ν_{12}, ν_{13}	ν_{23}	α_{11} $(10^{-6}/\text{K})$	α_{22}, α_{33} $(10^{-6}/\text{K})$	κ_{11} (W/mK)	κ_{22}, κ_{33} (W/mK)
181	10.3	7.17	2.39	0.28	0.43	0.02	22.5	4.6	0.7

for this case is chosen to be $\delta = 0.1\%$. In Table 5, in which pm-HLEn indicate a FE model with mth-order hierarchical element adopting n-th order HLE as thickness functions. As shown in Table 5, the order of the shape functions is first increased, then the order of the thickness functions are enhanced until the numerical convergence is achieved. The final results obtained for $R_\beta/h = 2, 10, 500$ are summarized in Table 6. For comparison purposes, the results obtained with nine-node Lagrangian elements (Q9) are also reported. For the thin shells with $R_\beta/h = 10$ and 500, to mitigate the shear and membrane locking phenomena, the Mixed Interpolation of Tensorial Components (MITC) technique is applied to Q9 elements, leading to MITC9 elements. First-order Shear Deformation Theory (FSDT) is also tested. The numerical efficiency of FE models is assessed through the number of degrees of freedom (DOFs) and the relative CPU time $\bar{t}$, which is measured by dividing the CPU time consumed by the single-element model $p2$-HLE1. The reference solutions were presented by Cinefra et al. [6]. Through-thickness variations of transverse stresses $\sigma_{\alpha z}$, $\sigma_{\beta z}$, and σ_{zz} are reported in Fig. 3, wherein the stresses for the cylindrical panels with $R_\beta/h = 500$ are amplified certain times for the convenience of observation.

From Table 5, it can be observed that the p-refinement is more convenient to conduct than the h-refinement. By simply increasing the order of the shape functions without re-meshing, the numerical accuracy can be improved. Meanwhile, the p-refinement requires a fewer number of increased DOFs in each enhancement step than h-refinement, which is more promising to lead to optimal numerical efficiency. Fig. 3 shows that the CUF-based refined shell FE models used in the present work are capable of giving numerical results with 3D accuracy.

As summarized in Table 6, the numerical results obtained with CUF-based refined FE models through the adaptive refinement are in agreement with those given by analytical solutions as presented by Cinefra et al. [6], and slight differences can be observed on the thick cylindrical panel with $R_\beta/h = 2$. Fig. 4 compares the temperature profiles through the thickness of the shells obtained by the coupled thermo-mechanical models and those provided by Cinefra et al. [6]. For the cylindrical panels with $R_\beta/h = 2$ and 10, the temperature profiles achieved in different approaches are marginally different.

It should be noted that in the coupled thermo-mechanical FE models in the present work,

Table 5: Displacement and stress estimations on the two-layered cylindrical panels with $R_\beta/h = 500$.

Mesh	N_i	F_τ	$w/10^{-3}$mm $(\frac{a}{2},\frac{b}{2},\frac{h}{2})$	$\sigma_{\alpha\alpha}$/KPa $(\frac{a}{2},\frac{b}{2},\frac{h}{2})$	$\sigma_{\beta\beta}$/KPa $(\frac{a}{2},\frac{b}{2},\frac{h}{2})$	$\sigma_{\alpha\beta}$/KPa $(a,b,-\frac{h}{2})$	$\sigma_{\alpha z}$/KPa $(a,\frac{b}{2},\frac{h}{4})$	$\sigma_{\beta z}$/KPa $(\frac{a}{2},b,\frac{h}{4})$	σ_{zz}/KPa $(\frac{a}{2},\frac{b}{2},0)$	DOFs	CPU time $\bar{t}$
1×1	$p2$	HLE1	6.552	-13645	595.2	-27.81	-44.45	-177.7	-5203	96	1.0
1×1	$p3$	HLE1	8.477	-13158	205.6	-54.58	-21.11	-101.7	-4959	144	1.0
1×1	$p4$	HLE1	8.327	-13244	-421.3	62.91	9.79	-11.15	-5113	204	1.1
1×1	$p5$	HLE1	8.314	-13271	-347.1	47.70	16.66	-1.065	-5157	276	1.1
1×1	$p6$	HLE1	8.330	-13272	-293.1	47.08	15.52	-2.457	-5157	360	1.2
1×1	$p7$	HLE1	8.327	-13271	-293.2	47.40	15.49	-2.500	-5156	456	1.3
1×1	$p8$	HLE1	8.327	-13271	-294.3	47.43	15.50	-2.481	-5156	564	1.4
1×1	$p9$	HLE1	8.327	-13271	-294.3	47.42	15.50	-2.481	-5156	684	1.6
1×1	$p9$	HLE2	8.227	-11024	1765	40.52	14.57	-2.803	9.468	1140	1.9
1×1	$p9$	HLE3	8.227	-11025	1764	40.52	15.07	-3.355	8.150	1596	2.3
1×1	$p9$	HLE4	8.227	-11025	1764	40.52	15.07	-3.355	8.160	2052	2.8
1×1	$p9$	HLE5	8.227	-11025	1764	40.52	15.07	-3.355	8.160	2508	3.3
5×5	MITC9	HLE5	8.228	-11020	1807	41.30	15.15	-3.385	8.263	5324	8.3
10×10	MITC9	HLE5	8.227	-11024	1775	40.69	15.10	-3.362	8.162	19404	24.3
1×1	$p9$	FSDT	1.933^{-4}	-2.046	-1.577	1.234×10^{-2}	1.017×10^{-3}	2.999×10^{-3}	–	380	1.4
Cinefra et al. (2017)(Analytical)			8.2246	-11025	–	–	15.070	–	–		

the temperature and displacement solutions are both treated as primary variables in the FE formulations and the equation system is solved in one step. While in the reference work [6], first the through-thickness temperature profile is achieved by solving the heat conduction equation through a combination of hyperbolic sine and cosine series, then in an *a priori* way, the 3D temperature field is obtained by means of multiplying the temperature profile by the in-plane bi-sinusoidal distribution. Such solutions do not work rigorously for thick curved structures.

FSDT fails in giving reasonable numerical approximations in the tested cases even for the thin cylindrical panel with $R_\beta/h = 500$ mainly due to its incapabilities in rendering the temperature distribution through the thickness. MITC9 elements with hierarchical Legendre expansions as thickness functions can achieve comparable accuracy as the hierarchical shell elements but at the cost of more DOFs and higher computational time consumption.

Table 6: Displacement and stress estimations on the two-layered cylindrical panels with various R_β/h values.

R_β/h	Mesh	N_i	F_τ	$w/10^{-3}$mm $(\frac{a}{2},\frac{b}{2},\frac{h}{2})$	$\sigma_{\alpha\alpha}$/KPa $(\frac{a}{2},\frac{b}{2},\frac{h}{2})$	$\sigma_{\beta\beta}$/KPa $(\frac{a}{2},\frac{b}{2},\frac{h}{2})$	$\sigma_{\alpha\beta}$/KPa $(a,b,-\frac{h}{2})$	$\sigma_{\alpha z}$/KPa $(a,\frac{b}{2},\frac{h}{4})$	$\sigma_{\beta z}$/KPa $(\frac{a}{2},b,\frac{h}{4})$	σ_{zz}/KPa $(\frac{a}{2},\frac{b}{2},0)$	DOFs	CPU time $\bar{t}$
2	1×1	$p7$	FSDT	0.3012	-393.7	371.2	149.7	2.233	-3.984	5.482	266	1.2
	1×1	$p7$	HLE8	16.91	-6923	9619	-44.79	529.4	-1112.0	271.9	2584	3.2
	5×5	Q9	HLE8	16.90	-6898	9709	-45.16	526.2	-1123	273.9	8228	5.3
	Cinefra et al. (2017)(Analytical)			16.403	-7073.4	–	–	541.76	–	–		
10	1×1	$p9$	FSDT	0.1999	-84.43	49.08	27.63	1.486	1.683	1.179	399	1.5
	1×1	$p9$	HLE5	18.67	-8934	8950	1113	545.4	-497.9	342.8	2508	3.4
	10×10	MITC9	HLE5	18.67	-8929	8975	1118	546.5	-499.0	343.9	19404	23.9
	Cinefra et al. (2017)(Analytical)			18.570	-8957.6	–	–	543.49	–	–		
500	1×1	$p9$	FSDT	1.933^{-4}	-2.046	-1.577	1.234×10^{-2}	1.017×10^{-3}	2.999×10^{-3}	–	399	1.4
	1×1	$p9$	HLE5	8.227	-11025	1764	40.52	15.07	-3.355	8.160	2508	3.3
	10×10	MITC9	HLE5	8.227	-11024	1775	40.69	15.10	-3.362	8.162	19404	24.3
	Cinefra et al. (2017)(Analytical)			8.2246	-11025	–	–	15.070	–	–		

(a) $\sigma_{\alpha z}$ $(a, \frac{b}{2}, \bar{z})$ (b) $\sigma_{\beta z}$ $(\frac{a}{2}, b, \bar{z})$ (c) σ_{zz} $(\frac{a}{2}, \frac{b}{2}, \bar{z})$
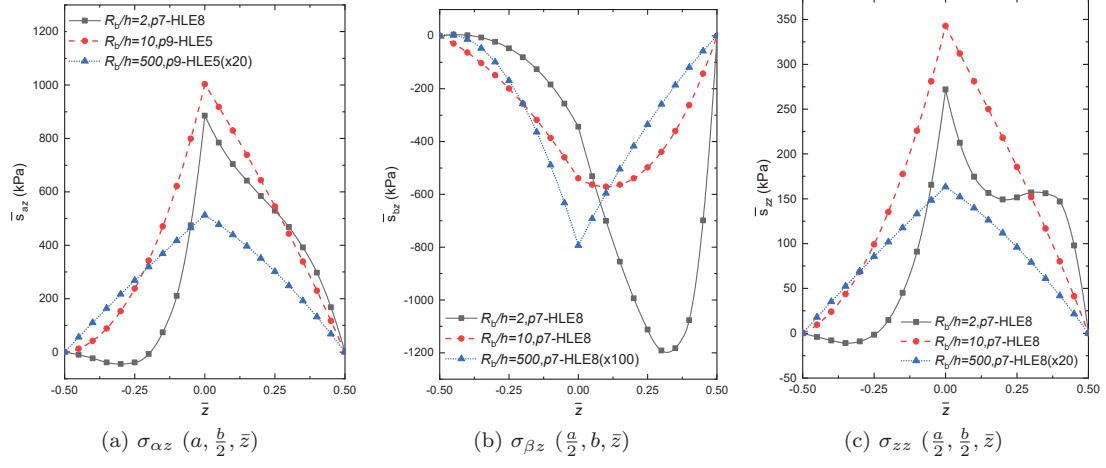
Figure 3: Through-thickness variation of transverse stresses on the two-layered cylindrical panels with imposed temperature on top and bottom surfaces. Radius-to-thickness ratios $R_\beta/h = 2$, 10, and 500, are considered. FE models adopt p-version shape functions and hierarchical Legendre expansions (HLE) as thickness functions.
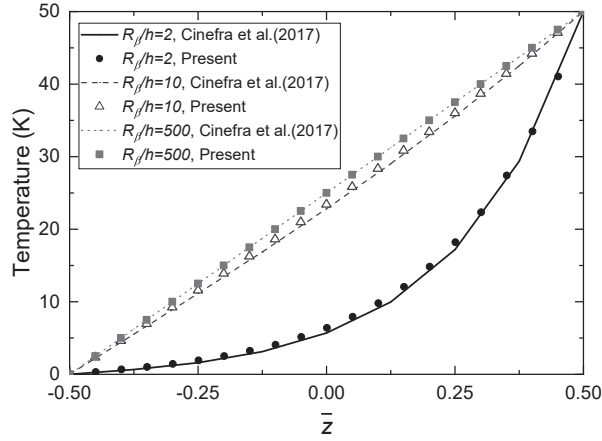

Figure 4: Through-thickness variation of temperature on the two-layered cylindrical panels with $R_\beta/h = 2$, 10, and 500. Numerical results obtained with the employed FE models are compared against the reference solutions.

5.4. A two-layered spherical shell under local distributed temperature

A two-layered laminated spherical shell with lamination sequence [0°/90°] under temperature imposed on the local region on the top surface is considered. The lamination sequence is [0°/90°] (from bottom to top), and the two layers have equal thickness. The shell has length and width $a = b = 0.1$m, radii $R = R_\alpha = R_\beta = 0.1$m, and radius-to-thickness ratio $R/h = 20$. The lamina properties are the same as in Table 4 in Section 5.3.

The local region covers $\frac{1}{5} \times \frac{1}{5}$ of the central area on the top surface, and the temperature distribution follows:

$$\theta_0(\alpha, \beta, \frac{h}{2}) = \theta_M \cdot \sin(\frac{\pi\alpha}{5a})\sin(\frac{\pi\beta}{5b}) \qquad \alpha \in \left[\frac{2a}{5}, \frac{3a}{5}\right], \beta \in \left[\frac{2a}{5}, \frac{3b}{5}\right]. \tag{41}$$

where the magnitude of the temperature is θ_M=50K. On the bottom surface and in the rest area on the top surface, the temperature is constrained to be zero. The boundary conditions on the edges are set according to Eqn. 39.

A quarter of the structure is models with 5×5 hierarchical shell elements with the help of symmetric boundary conditions. Fist of all, the kinematic model is set to be FSDT, and the order of the hierarchical elements is increased. Secondly, the local region which covers only one element is simulated with refined LW models adopting progressively refined LW models with HLE and the non-critical area modeled with FSDT, leading to FE models denoted as FSDT-HLE$n^{\times 1}$, see Fig. 5(a). And then, the locally refined region is expanded to the range of 2×2 elements, and the corresponding FE models are represented by FSDT-HLE$n^{\times 4}$, as illustrated in Fig. 5(b). Finally, in the non-critical area, the employed kinematics is switched to ESL models adopting TE2 (second-order Taylor Expansions). Considering the in-compatibility of LW and ESL models, the threshold of the relative difference between two rounds is chosen to be $\delta \leq 10.0\%$, which lead to a reasonable estimation of most of the stresses.

The results obtained are summarized in Table 7. Note that the relative CPU time reported is measured with reference to the time consumption of the model $p2$-FSDT, similarly to the previous case in Section 5.3. From Table 7, it can be observed that eighth-order elements can give good in-plane approximations, and HLE5 used on the 2×2 local region can lead to reasonably good estimation of the structural responses. The refinement of kinematic models in the outlying zone can also help to improve simulation accuracy. The NDK model TE2-HLE5$^{\times 4}$ provides comparable accuracy with the uniformly refined model HLE5, yet with a significantly reduced number of DOFs and CPU time consumption. Figs. 6 and 7 compare the temperature and $\sigma_{\alpha z}$
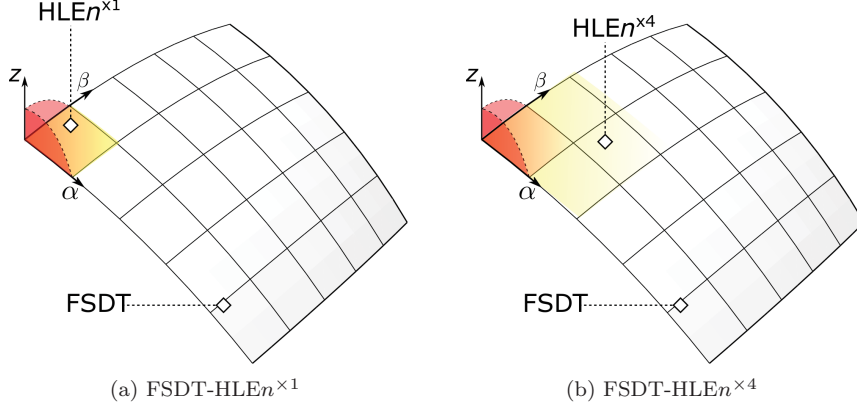
17

(a) FSDT-HLE$n^{\times 1}$ (b) FSDT-HLE$n^{\times 4}$

Figure 5: FE models with variable FSDT/HLEn nodal kinematics for the two-layered cylindrical shell under local distributed temperature. The region with nth-order HLE thickness functions in FE model (a) covers one element; in FE model (b) it covers four elements.

Table 7: Displacement and stress evaluations for the two-layered spherical shell with $R/h = 20$ under local distributed temperature.

N_i	F_τ	$w/10^{-3}\mathrm{mm}$ $\left(\frac{a}{2},\frac{b}{2},\frac{h}{2}\right)$	$\sigma_{\alpha\alpha}/\mathrm{KPa}$ $\left(\frac{a}{2},\frac{b}{2},\frac{h}{2}\right)$	$\sigma_{\beta\beta}/\mathrm{KPa}$ $\left(\frac{a}{2},\frac{b}{2},\frac{h}{2}\right)$	$\sigma_{\alpha\beta}/\mathrm{KPa}$ $\left(\frac{23a}{40},\frac{23b}{40},-\frac{h}{2}\right)$	$\sigma_{\alpha z}/\mathrm{KPa}$ $\left(a,\frac{11b}{20},\frac{h}{4}\right)$	$\sigma_{\beta z}/\mathrm{KPa}$ $\left(\frac{11a}{20},b,\frac{h}{4}\right)$	σ_{zz}/KPa $\left(\frac{a}{2},\frac{b}{2},0\right)$	DOFs	CPU time $\bar{t}$
$p2$	FSDT	0.01522	-38.11	45.36	-3.378	0.6302	1.556	0.1068	672	1.0
$p3$	FSDT	0.01511	-37.64	39.41	-3.689	0.2622	0.3914	0.1494	1092	2.5
$p4$	FSDT	0.01532	-39.91	32.90	-3.972	0.1487	0.06048	0.2575	1687	4.2
$p5$	FSDT	0.01539	-40.11	33.01	-4.026	0.1251	-0.00423	0.2621	2457	6.0
$p6$	FSDT	0.01540	-39.97	33.59	-4.060	0.1384	0.03509	0.2548	3402	6.3
$p7$	FSDT	0.01540	-39.96	33.59	-4.070	0.1374	0.03198	0.2538	4522	9.9
$p8$	FSDT	0.01540	-39.96	33.58	-4.072	0.1374	0.03204	0.2542	5817	15.4
$p8$	FSDT-HLE1$^{\times 1}$	4.357	-10134	5523	-1240	511.5	-446.5	-2933	6052	15.5
$p8$	FSDT-HLE2$^{\times 1}$	4.049	-8440	7760	-1044	441.7	-298.8	-107.8	6428	16.5
$p8$	FSDT-HLE3$^{\times 1}$	4.092	-7997	8403	-1047	422.8	-477.4	80.48	6804	18.2
$p8$	FSDT-HLE4$^{\times 1}$	4.092	-7952	8420	-1048	422.9	-476.3	117.6	7180	19.1
$p8$	FSDT-HLE5$^{\times 1}$	4.094	-7930	8423	-1048	421.2	-470.3	110.4	7556	20.9
$p8$	FSDT-HLE5$^{\times 4}$	4.104	-7902	8501	-1065	439.7	-470.7	103.8	11478	36.1
$p8$	TE2-HLE5$^{\times 4}$	4.108	-7889	8420	-1055	439.9	-465.7	110.9	10713	45.9
$p8$	HLE5	4.106	-7889	8480	-1055	439.8	-463.1	115.1	36564	175.3

18

obtained with the uniformly refined FE model HLE5 and TE2-HLE5$^{\times 4}$, respectively. It can be observed that both the temperature and stress fields obtained with different FE models agree well.

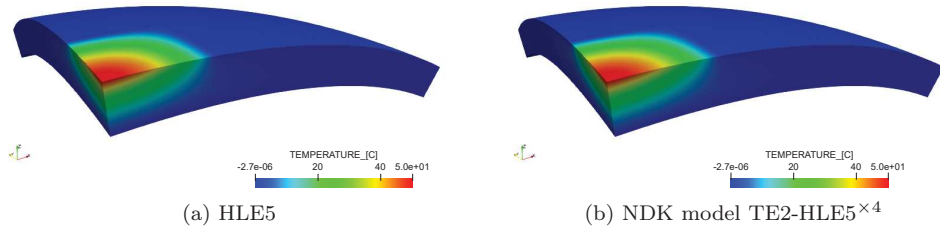(a) HLE5   (b) NDK model TE2-HLE5$^{\times 4}$

Figure 6: Numerical estimations of temperature (K) distribution for the two-layered spherical shell with $R/h = 20$ under local distributed temperature, obtained with 5×5 $p8$ elements. In (a), HLE5 thickness functions are uniformly used for all shape functions; in (b), only shape functions in the local critical region covering four elements are allocated to HLE5 thickness functions, and the outlying are adopts TE2 kinematic assumptions.
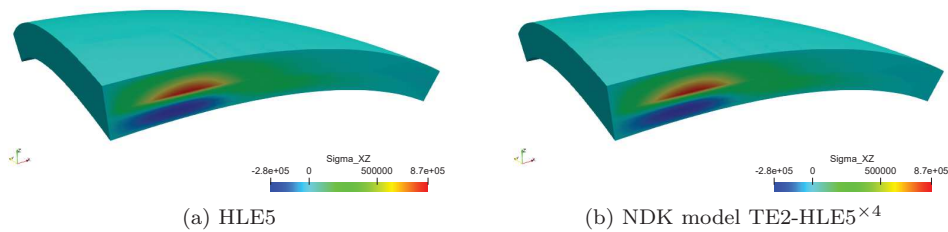

(a) HLE5   (b) NDK model TE2-HLE5$^{\times 4}$

Figure 7: Numerical estimations of $\sigma_{\alpha z}$(Pa) for the two-layered spherical shell with $R/h = 20$ under local distributed temperature, obtained with 5×5 $p8$ elements. In (a), HLE5 thickness functions are uniformly used for all shape functions; in (b), only shape functions in the local critical region covering four elements are allocated to HLE5 thickness functions, and the outlying are adopts TE2 kinematic assumptions.

6. Conclusions

Coupled thermo-mechanical shell finite element models with Node-Dependent Kinematics (NDK) for steady-state problems are presented. The coupled thermo-mechanical shell models can give the temperature variation and displacement solutions directly in a one-step manner. Through numerical examples on composite laminated shell structures, an adaptable refinement approach based on NDK is demonstrated, and the numerical accuracy and efficiency of the NDK FE models are assessed.

- For thick curved structures, the coupled thermo-mechanical models can provide more appropriate solutions compared to a two-step procedure (firstly obtain the temperature profile

19

through the thickness, then substitute the thickness profile into the thermal stress calculation).

- The mathematical enhancement of FE models, namely the refined kinematics assumption over the shell thickness and the increase of the order of the p-version elements, empowers one to fully utilize the capabilities of a given set of 2D mesh grids in obtaining accurate structural responses with quasi-3D accuracy.

- The use of NDK makes it convenient to improve the numerical accuracy with balanced computation costs.

This adaptive refinement approach requires the minimum level of re-meshing work and is promising to help increase the efficiency of engineering simulations. It can be further extended to other situations such as plasticity and damage modeling, delamination simulations, and contact analyses.

7. Acknowledgment

References

[1] E. Carrera. Temperature profile influence on layered plates response considering classical and advanced theories. *AIAA Journal*, 40(9):1885–1896, 2002.

[2] E. Carrera and E. Zappino. One-dimensional finite element formulation with node-dependent kinematics. *Computers & Structures*, 192:114–125, 2017.

[3] E. Carrera, M. Cinefra, and F. A. Fazzolari. Some results on thermal stress of layered plates and shells by using unified formulation. *Journal of Thermal Stresses*, 36(6):589–625, 2013.

[4] E. Carrera, M. Cinefra, M. Petrolo, and E. Zappino. *Finite element analysis of structures through Unified Formulation*. John Wiley & Sons, 2014.

[5] M. Cinefra, S. Valvano, and E. Carrera. Heat conduction and thermal stress analysis of laminated composites by a variable kinematic MITC9 shell element. *Curved and Layered Structures*, (1):301–320, 2015.

[6] M. Cinefra, M. Petrolo, G. Li, and E. Carrera. Variable kinematic shell elements for composite laminates accounting for hygrothermal effects. *Journal of Thermal Stresses*, 40(12): 1523–1544, 2017.

[7] Y. Das and B. Rath. Thermal bending of moderately thick rectangular plate. *AIAA Journal*, 10(10):1349–1351, 1972.

[8] P. Dumir, J. Nath, P. Kumari, and S. Kapuria. Improved efficient zigzag and third order theories for circular cylindrical shells under thermal loading. *Journal of Thermal Stresses*, 31(4):343–367, 2008.

[9] A. Düster, H. Bröker, and E. Rank. The p-version of the finite element method for three-dimensional curved thin walled structures. *International Journal for Numerical Methods in Engineering*, 52(7):673–703, 2001.

[10] J. Fourier. *Theorie analytique de la chaleur, par M. Fourier*. Chez Firmin Didot, père et fils, 1822.

[11] M. T. Hicks. Design of a carbon fiber composite grid structure for the glast spacecraft using a novel manufacturing technique. Technical report, SLAC, 2001.

[12] F. Jacquemin and A. Vautrin. A closed-form solution for the internal stresses in thick composite cylinders induced by cyclical environmental conditions. *Composite Structures*, 58 (1):1–9, 2002.

[13] T. Kant and R. Khare. Finite element thermal stress analysis of composite laminates using a higher-order theory. *Journal of Thermal Stresses*, 17(2):229–255, 1994.

[14] S. Kapuria, S. Sengupta, and P. Dumir. Three-dimensional solution for a hybrid cylindrical shell under axisymmetric thermoelectric load. *Archive of Applied Mechanics*, 67(5):320–330, 1997.

[15] R. K. Khare, T. Kant, and A. K. Garg. Closed-form thermo-mechanical solutions of higher-order theories of cross-ply laminated shallow shells. *Composite Structures*, 59(3):313–340, 2003.

[16] A. Khdeir. Thermoelastic analysis of cross-ply laminated circular cylindrical shells. *International Journal of Solids and Structures*, 33(27):4007–4017, 1996.

[17] A. Khdeir and J. Reddy. Thermal stresses and deflections of cross-ply laminated plates using refined plate theories. *Journal of Thermal Stresses*, 14(4):419–438, 1991.

[18] A. A. Khdeir, M. D. Rajab, and J. N. Reddy. Thermal effects on the response of cross-ply laminated shallow shells. *International Journal of Solids and Structures*, 29(5):653–667, 1992.

[19] G. Kulikov and S. Plotnikova. Heat conduction analysis of laminated shells by a sampling surfaces method. *Mechanics Research Communications*, 55:59–65, 2014.

[20] A. W. Leissa. *Vibration of shells*, volume 288. Scientific and Technical Information Office, National Aeronautics and Space Administration Washington, 1973.

[21] G. Li. *Variable Kinematic Finite Element Formulations Applied to Multi-layered Structures and Multi-field Problems*. PhD thesis, Ph. D. thesis. Torino, italy: Politecnico di Torino, Department of Mechanical and Aerospace Engineering, 2019.

[22] G. Li, E. Carrera, M. Cinefra, A. de Miguel, A. Pagani, and E. Zappino. An adaptable refinement approach for shell finite element models based on node-dependent kinematics. *Composite Structures*, 210:1–19, 2019.

[23] C. J. Miller, T. Kicher, and W. Millavec. Thermal stress analysis of layered cylindrical shells. *AIAA Journal*, 19(4):523–530, 1981.

[24] J. Reddy. A simple higher-order theory for laminated composite plates. *Journal of Applied Mechanics*, 51(4):745–752, 1984.

[25] J. Reddy. *Mechanics of laminated composite plates and shells: theory and analysis*. CRC Press, 2004.

[26] J. Reddy and C. Liu. A higher-order shear deformation theory of laminated elastic shells. *International Journal of Engineering Science*, 23(3):319–330, 1985.

[27] J. N. Reddy. *Energy and variational methods in applied mechanics: with an introduction to the finite element method*. Wiley New York, 1984.

[28] C. Schwab. *P-and Hp-Finite Element Methods: Theory and Applications in Solid and Fluid Mechanics (Numerical Mathematics and Scientific Computation).* Oxford University Press, New York, 1999.

[29] M. Suri. Analytical and computational assessment of locking in the hp finite element method. *Computer Methods in Applied Mechanics and Engineering*, 133(3-4):347–371, 1996.

[30] B. Szabó, A. Düster, and E. Rank. *The p-Version of the Finite Element Method.* Wiley Online Library, 2004.

[31] B. A. Szabó. Mesh design for the p-version of the finite element method. *Computer Methods in Applied Mechanics and Engineering*, 55(1-2):181–197, 1986.

[32] B. A. Szabó and I. Babuška. *Finite element analysis.* John Wiley & Sons, 1991.